Study of nano-wire spin-Hall nano-oscillators

Bachelor thesis

Tim Bexter, WWU Münster
Student no. 380345

Supervisor
Prof. Dr. Sergej Demokritov

Münster, August 2015

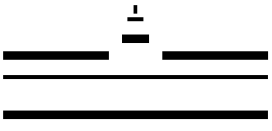

Westfälische
Wilhelms-Universität
Münster

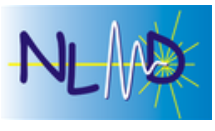

1. Gutachter: Prof. Dr. S. O. Demokritov
2. Gutachter: Dr. V. E. Demidov

Abstract

The topic of this thesis is the excitation of magnetization self-oscillations in a magnetic nano-wire by spin-Hall effect.
The fundamental equation in magnetics, the Landau-Lifshitz-Gilbert equation results in a precession movement of the magnetization if the system loses it's equilibrium. In this thesis this precession movement will be excited by a spin current originating from the spin-Hall effect, which will act as negative damping exceeding the Gilbert damping.
In the first part the experiment itself is demonstrated. Different harmonic modes of oscillation movement are observed and characterized with varying parameters, finding the optimal parameters for the excitation of magnetization oscillations. It is shown that magnetization oscillations can be excited in a one-dimensional structure with the usage of spin-Hall effect.
As a second part micromagnetic simulations are calculated. Two different mode regimes are found, edge and bulk mode, and the oscillations in the experiment are identified as edge modes. Spatial profiles of the oscillation movements are obtained and discussed.

Contents

List of Figures

1 Introduction

Today's every day life is characterized by electronic devices. With the growing need for data volume memory device research has become an important research field. The magnetization direction of magnetic particles is for example used as information storage by modern memory devices like hard drives. As a result the fundamental physics behind magnetic nanostructures are worth researching, as for example the discovery of the giant magnetoresistance (GMR) by Fert and Grünberg [3] [4] (Nobel Prize in Physics 2007) and later the tunnel magnetoresistance (TMR) [5] showed when they were introduced in the field of magnetic field sensors.
With the discovery of these effects depending on the spin orientation of electrons the research field of spintronics rose with the aim of carrying information without an electric current solely by spin waves. These spin waves were first introduced as concept by Bloch in 1930 [6] as part of his research about the temperature dependence on the magnetization in ferromagnets. Spin waves describe coherent precession movements of the magnetic moments in a magnetic material. They show typical wave phenomena as propagation, reflectiom, refraction and interference [7].
In this work the excitation of spin waves with a spin transfer torque (STT) in a permalloy ($Ni_{80}Fe_{20}$) nano-wire by spin-Hall effect is studied. Spin torque oscillations (STO) have already been observed in various nanoscale devices [8] [9]. However, in these studies the region where STO could be observed was restricted to the nanoscale and in a magnetic film as two-dimensional system no STO could be observed [10]. A nano-wire forms the intermediate structure between a nanoscale region and a two-dimensional film as a one-dimensional structure.
STT by spin-Hall effect qualifies as excitation method since magnetization movements can be controlled over a large region and without sending a current directly into the magnetic material.
Permalloy, being based on metal, is a ferromagnet with low magnetic losses (high magnetic permeability) and can be integrated into conventional semiconductor devices, what makes it a suitable material for research purposes and application.
The typical behavior of spin waves in confined structures consists of building two eigenmode regimes that are often called edge and bulk mode with respect to their localization. This is caused by demagnetizing effects at the samples boundaries [11].
In the beginning of this thesis the theoretical framework of magnetization dynamics and spin-Hall effect will be introduced in chapter 2. The sample used in the experiment and the experimental setup are described in chapter 3. In chapter 4 the experimental results are presented. A numeric simulation model for the sample is observed in chapter 5. All findings are summarized and discussed in chapter 6.

2 Theoretical Framework

In this chapter a brief overview about the theoretical basics of magnetization dynamics is given. First fundamental theory in form of the Landau-Lifshitz equation is presented. Subsequently the ferromagnetic resonance is introduced as important phenomena for the experimental method followed by explanations of spin waves and spin-Hall effect.

2.1 Fundamental Considerations

Static Magnetization The magnetic characteristics of ferromagnetic materials are caused by the exchange interaction of their electron spins $\vec{S}$ [12]. This exchange interaction results from the Pauli exclusion principle and coulomb interaction and therefore has quantum mechanical origins. Accordingly it is described by the Heisenberg Exchange Hamiltonian between two electron spins $\vec{S}_i$ and $\vec{S}_k$

$$\mathcal{H}_{\text{Heis}} = -J\vec{S}_i \cdot \vec{S}_k \tag{1}$$

with the exchange constant J. In order to minimize the energy this exchange interaction favors an alignment of parallel (or anti parallel for $J < 0$) spins.
Additionally every spin is connected to a magnetic moment $\vec{\mu}$ given by

$$\vec{\mu}_i = -g\mu_{\text{B}}\vec{S}_i \tag{2}$$

with the Lande factor g of the electron and the Bohr magneton $\mu_{\text{B}} = \frac{e\hbar}{2m_e}$ with the reduced Planck constant $\hbar$, the electron charge e and the electron mass m_e. Due to the parallel alignment of spins this leads to a macroscopic magnetization first introduced by Herring and Kittel [13] to describe the macroscopic behavior of a ferromagnet in a unit volume V of the magnet:

$$M = \frac{1}{V}\sum_i \mu_i. \tag{3}$$

For temperatures below the Curie point [14] and on a microscopic scale the magnetization can be found originating from a spontaneous aligning of the electron magnetic moments while on a macroscopic scale domain structures of parallel spins are formed, that minimize the free energy. For higher temperatures the magnetic moments follow thermal statistics and cancel each other out. Applying an external magnetic field $\vec{H}$ makes the magnetic moments align parallel to the field direction, until for a strong enough field a saturation magnetization $\vec{M}_0$ is achieved.

Motion of Magnetization Since the magnetic moment is connected to the angular momentum by $\vec{\mu} = -\gamma\vec{L}$ with the gyromagnetic ratio $\gamma = \frac{g\mu_B}{\hbar}$ it can be changed by a torque $\vec{T}$ acting on it:

$$\frac{d\vec{L}}{dt} = \vec{T}. \tag{4}$$

Following [15] we now want to consider the dynamics of a magnetic system. In magnetics the torque acting on the system is given by a magnetic external field H with

$$\vec{T} = \vec{\mu} \times \vec{H}. \tag{5}$$

With the magnetization as sum over all magnetic moments one gets the Landau-Lifshitz equation (short LLE) [12]

$$\frac{\partial\vec{M}}{\partial t} = -\gamma\vec{M} \times \vec{H}. \tag{6}$$

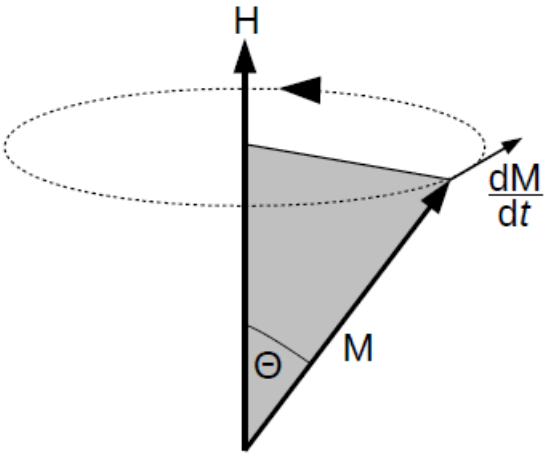

Figure 1: Precession of the magnetization around the magnetic field as given by the LLE. Taken from [1].

From the LLE we can see, either by simply acknowledging the fact that $\frac{\partial\vec{M}}{\partial t}$ stands perpendicular on both $\vec{M}$ and $\vec{H}$, or by scalar multiplicating the LLE with M [12], getting

$$\frac{\partial M^2}{\partial t} = 0 \tag{7}$$

that the systems movement is a precession of $\vec{M}$ with $|\vec{M}| = \text{const.}$ (figure 1). With the energy provided by the magnetic field one can follow

$$\omega = \gamma H. \tag{8}$$

Since other physical effects besides the external field can influence the system, instead of H an effective field H_{eff} can be used [15]

$$H_{\text{eff}} = H_{\text{ext}} + H_{\text{d}} + H_{\text{ex}} + H_{\text{a}} \tag{9}$$

that can consist of:

- the external field H_{ext} and the resulting Zeeman energy,
- the dipole field H_{d}, which results from the dipole-dipole interaction between the different magnetic moments in the sample,
- the exchange field H_{ex}, which is given by the exchange energy,
- the anisotropy field H_{a} taking in account anisotropies in the magnetic sample.

For a translationally noninvariant system the dipole part H_{d} must be considered because the density of the magnetic moments is not uniform, resulting in nonuniform magnetic charge densities ρ_{M}. When the magnetic moments have a component perpendicular to the magnetic materials surface, they create magnetic charges. These magnetic charges create the demagnetizing field, that reduces the effective field [16]. We call this the internal field H_{int}:

$$H_{\text{int}} = H_{\text{ext}} - H_{\text{demag}}. \tag{10}$$

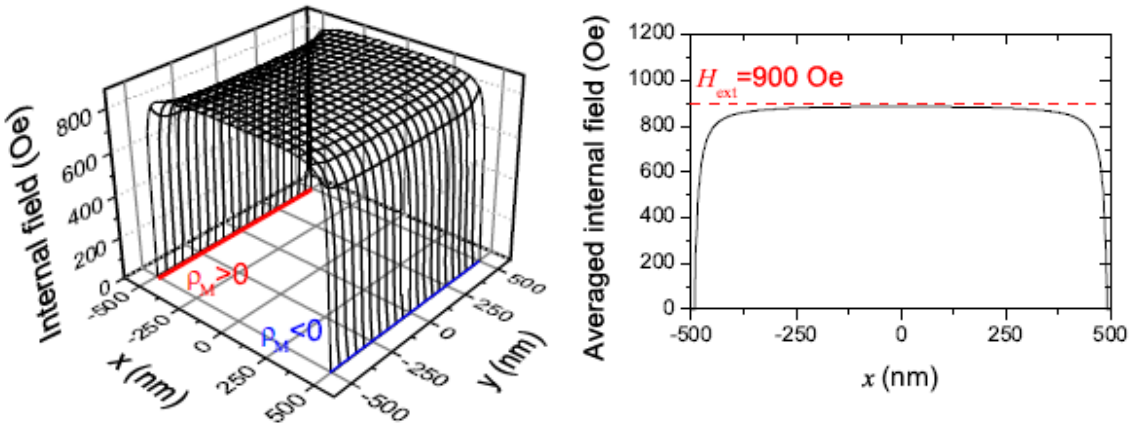

Figure 2: The internal field H_{int} of a thin Py sample (size: $1000\,nm \times 1000\,nm \times 5\,nm$). Left: x-component of H_{int}, the red and blue lines mark the magnetic charge densities at the edges. Right: avered field along the x-direction. Both figures taken from [2].

The demagnetizing field depends on the sample shape and can be calculated by the demagnetizing tensor N. For a rotational ellipsoid every off-diagonal element vanishes and the precession frequency can be calculated using the Kittel formula:

$$\omega = \gamma \sqrt{\left[H_{\text{ext}} + (N_x - N_z)\, M\right] \cdot \left[H_{\text{ext}} + (N_y - N_z)\, M\right]} \tag{11}$$

with the external field in z-direction. For example for an in-plane magnetized thin film one gets $N_\mathrm{x} = 4\pi$ and $N_\mathrm{y} = N_\mathrm{z} = 0$. Then the frequency is given by

$$\omega = \gamma\sqrt{H_\mathrm{ext}\,(H_\mathrm{ext} + 4\pi M)}. \tag{12}$$

Damping and the Gilbert Factor Since the LLE only describes a system without damping, a damping torque pointing towards the static magnetic field can be added to include losses. It becomes the Landau-Lifshitz-Gilbert equation (LLGE)

$$\frac{\partial\vec{M}}{\partial t} = -\gamma\vec{M}\times\vec{H}_\mathrm{eff} - \frac{\alpha_\mathrm{G}}{M_0}\vec{M}\times\frac{\partial\vec{M}}{\partial t} \tag{13}$$

with the Gilbert damping parameter α_G giving the strength of the damping, but not any information about its nature.

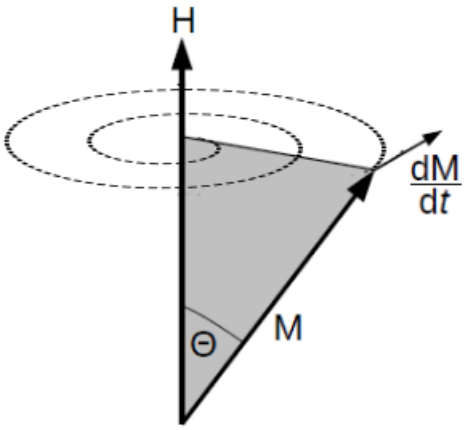

Figure 3: Precession of the magnetization around the magnetic field including damping.

2.2 Dynamic Magnetic Susceptibility and Ferromagnetic Resonance

To consider the systems reaction to a dynamic magnetic field we follow [12] using the dynamic field and magnetization

$$\vec{H} = \vec{H}_0 + \vec{h}_\sim \qquad\qquad \vec{M} = \vec{M}_0 + \vec{m}_\sim \tag{14}$$

with the constant $\vec{H}_0 \parallel \vec{M}_0$ in z-direction and the dynamic components

$$h_\sim \ll H_0 \qquad \text{and} \qquad m_\sim \ll M_0. \tag{15}$$

Solving the LLE with these assumptions one gets

$$\vec{m}_{\sim} = \hat{\chi} \cdot \vec{h}_{\sim} \qquad \text{with} \qquad \hat{\chi} = \begin{pmatrix} \chi & i\chi_a & 0 \\ -i\chi_a & \chi & 0 \\ 0 & 0 & 0 \end{pmatrix}. \tag{16}$$

$\hat{\chi}$ is the dynamic susceptibility tensor with

$$\chi = \frac{\gamma^2 M_0 H_0}{(\gamma H_0)^2 - \omega^2} \qquad \text{and} \qquad \chi_a = \frac{\gamma M_0 \omega}{(\gamma H_0)^2 - \omega^2}. \tag{17}$$

For the characteristic frequency $\omega_H = \gamma H_0$ the components of the susceptibility tensor diverge (figure 4). This phenomenon is described as ferromagnetic resonance (FMR).

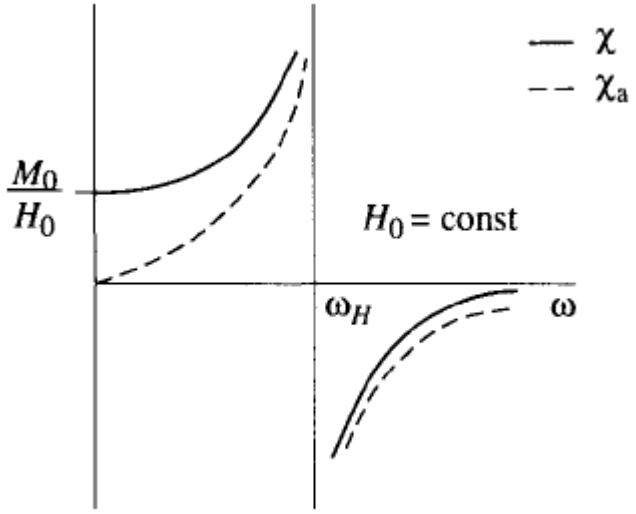

Figure 4: Components of the susceptibility tensor. Taken from [12].

To take damping into account one must add the Gilbert torque to the LLE (section 2.1). The solution for the LLGE can simply obtained by replacing H_0 with $H_0 + \frac{i\alpha\omega}{\gamma}$. The susceptibility tensor components then both become complex numbers

$$\chi = \chi' - i\chi'' \qquad \text{and} \qquad \chi_a = \chi_a' - i\chi_a''. \tag{18}$$

with the real and imaginary parts

$$\chi' = \gamma^2 M_0 H_0 \frac{(\gamma H_0)^2 - (1-\alpha^2)\,\omega^2}{\left[(\gamma H_0)^2 - (1+\alpha^2)\,\omega^2\right]^2 + 4\alpha^2\omega^2\,(\gamma H_0)^2} \tag{19}$$

$$\chi'' = \alpha\gamma M_0 \omega \frac{(\gamma H_0)^2 + (1+\alpha^2)\,\omega^2}{\left[(\gamma H_0)^2 - (1+\alpha^2)\,\omega^2\right]^2 + 4\alpha^2\omega^2\,(\gamma H_0)^2} \tag{20}$$

$$\chi'_a = \gamma M_0 \omega \frac{(\gamma H_0)^2 - (1+\alpha^2)\,\omega^2}{\left[(\gamma H_0)^2 - (1+\alpha^2)\,\omega^2\right]^2 + 4\alpha^2\omega^2\,(\gamma H_0)^2} \tag{21}$$

$$\chi''_a = \frac{2\alpha\omega^2\gamma^2 M_0 H_0}{\left[(\gamma H_0)^2 - (1+\alpha^2)\,\omega^2\right]^2 + 4\alpha^2\omega^2\,(\gamma H_0)^2} \tag{22}$$

$$\tag{23}$$

In this case the characteristic frequency becomes $\omega_H = \frac{\gamma H_0}{\sqrt{1+\alpha^2}}$ and the susceptibility tensor components no longer diverge. Instead the real parts of the components change their sign while the imaginary parts have a maximum at ω_H (figure 5). This results in the ferromagnetic resonance (FMR), a strong absorption of electromagnetic energy at the resonant frequency.

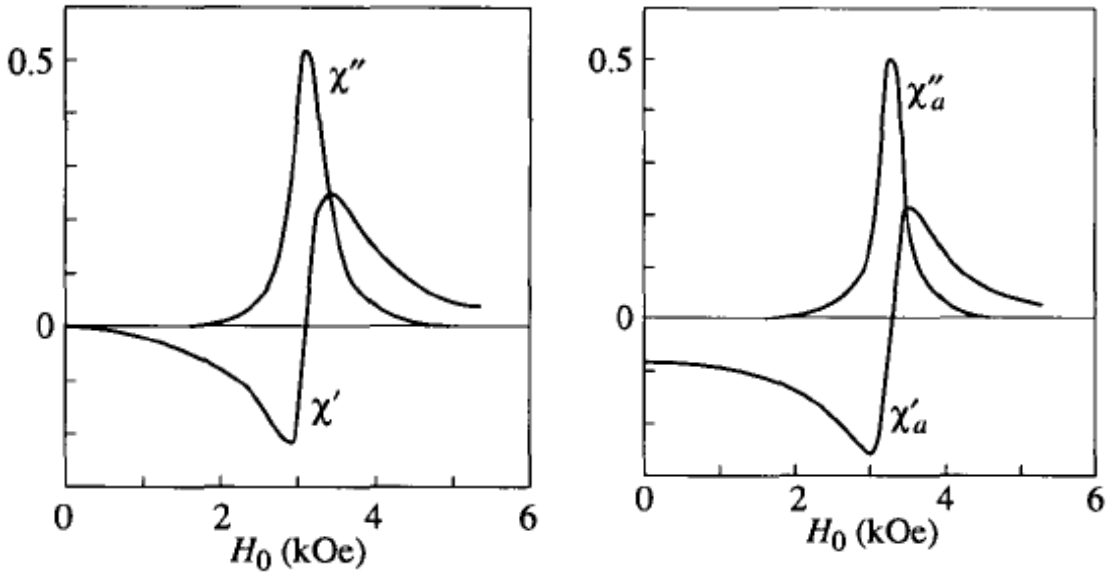

Figure 5: Components of the susceptibility tensor including damping. Taken from [12].

2.3 Spin Waves

Up to this point, we only considered a uniform precession movement of the magnetization in the whole magnet. However, of course it is also possible that the precession movement is nonuniform, for example because of a local excitation. In this case the magnetic moments are no longer parallel to each other and so energy is transferred from one to another by the dipolar and exchange interaction. For the calculation of

the dipolar energy contribution to $\vec{H}$ one can introduce a magnetic charge density $\rho_m = -\nabla\vec{M}$. For a magnetization $\vec{M}$ with a static component $\vec{M}_0$ and a small dynamic component $\vec{m}_\sim$ we can see from the Maxwell equation:

$$0 = \vec{\nabla}\left(\vec{H} + 4\pi\vec{M}\right) = \vec{\nabla}\left(\vec{h}_\sim + 4\pi\vec{m}_\sim\right) \tag{24}$$

$$\vec{h}_\sim = -4\pi\vec{m}_\sim = -\rho_m \neq 0. \tag{25}$$

This dynamic magnetization can be considered as a plane „spin wave“ in the form of $\vec{m} = \vec{m_0}\exp(-i\ \vec{\mathrm{k}}\ \cdot\ \vec{\mathrm{r}})$ with the wave vector $\vec{k}$. One can easily see that the case of uniform precession is the special case with $\vec{k} = 0$.
The first introduction of a dispersion law was made by Bloch [6], only taking the exchange interaction into account. With an linear approximation Kalinkos and Slavin [17] found the dispersion law including exchange and dipolar interaction to be

$$\omega^2(k) = \left(\omega_H + l_{ex}^2\omega_M k^2\right)\left(\omega_H + l_{ex}^2\omega_M k^2 + \omega_M + \sin^2\theta_k\right) \tag{26}$$

with the frequencies $\omega_H = \gamma H$ and $\omega_M = \gamma\mu_0 M_0$, the angle θ_k between M and k and the exchange length $l_{ex} = \sqrt{\frac{J}{2\pi M_0^2}}$ with the exchange constant J.
We can see that for internal magnetic fields with $H_{int} > 0$ the frequency increases quadratically with k. Furthermore there is a minimal frequency at $k = 0$ which depends on H_{int}. Spin waves excited with frequencies below that minimum will be damped exponentially. As a result, for inhomoheneous H_{int} at different points in a ferromagnetic sample different spin wave-frequencies can be found.

2.4 Spin Wave Mode Localization

As already mentioned in section 2.1 the dipolar exchange interaction results in a demagnetizing field H_{demag} that is spatially nonuniform for finite structures [16]. Considering the dispersion relation from above (26) in combination with the nonuniform field H_{int} one can see that the minimum frequency for a spin wave to not be disallowed by the dispersion relation is also spatially nonuniform, meaning that at different points in the sample different eigenmodes can exist. Since the demagnetizing field strongly reduces the internal field at the samples edges in field direction but nearly vanishes in the center regions (III) one can distinguish edge and center modes.
The confinement in a finite structure leads to a quantization of the wave vector. In the case of a plane wave with $\vec{m} = \vec{m}_0\exp(i\mathrm{k_x}x + i\mathrm{k_y}y)$ this quantization leads to

$$k_{mn} = \left[\frac{(m+1)\pi}{l_x}, \frac{(n+1)\pi}{l_y}\right] \tag{27}$$

where l_x and l_y are the side lengths of the sample. While for center modes, assuming local validity of the dispersion law [17], this already gives a good assumption neglecting the strong field reduction at the edge regions, edge modes can only exist in the two edge regions with width Λ_1 and $\Lambda_2 < l_x$ (assuming a magnetic field in x direction):

$$k_{mn} = \left[\frac{(m+1)\pi}{\Lambda}, \frac{(n+1)\pi}{l_y}\right] \tag{28}$$

As a result in a confined structure there can be found two different eigenmodes, the edge and the center mode.

2.5 Spin Wave Excitation ~~with~~ Spin-Hall Effect

In this section we will take a brief look at the spin-Hall effect (SHE) and how one can use it to excite magnetization dynamics. First theoretical considerations were made by Dyakonov and Perel [18] concerning semiconductors, later being extended to paramagnetic ~~materials~~ by Hirsch [19].

If a charge current $\vec{j}_c$ of unpolarized electrons scatters at a potential influenced by spin-orbit coupling the spin orientation gives the direction of the electron deflection. This leads to a spin current $\vec{j}_s$ perpendicular to $\vec{j}_c$. There are various numbers of physical mechanisms leading to SHE being distinguished between intrinsic and extrinsic SHEs [20].

For a complete description one would have to view the spin current as a tensor, because the spin current has to be considered as well as the magnetic moment. However, in this thesis only spin currents flowing in one direction are of interest, so j_s will be only scalar.

The spin-Hall angle Θ_{SH} gives the efficiency of the conversion from charge- to spin current and is dependent on the material. It is given by the charge conductivity $\sigma_c = ne\mu$ and the spin Hall conductivity $\sigma_s = n\hbar\mu\Theta_{\mathrm{SH}}$ with the electron mobility μ and electron density n to be [20]

$$\Theta_{\mathrm{SH}} = \frac{\sigma_s e}{\sigma_c \hbar}. \tag{29}$$

For platinum [21] found $\Theta_{\mathrm{SH}} = 0.076$, however there are several different methods to find Θ_{SH} with results differing by one order of magnitude [20].

When combining a material with spin-orbit coupling and a magnetic material one can use the SHE to excite magnetization dynamics. The spin current will diffuse in the magnetic layer, exerting a spin-transfer torque (STT) on the magnetization. The spatial scale in which STT is induced in the magnetic layer is limited by spin diffusion and spin dephasing [22]. As a result the STT is only exerted to a length of a few atomic layers into the magnetic material. For very thin magnetic layers, like nano-wires, we can still assume a homogeneous excitation.

This STT acting on the magnetization can be described by the Slonczewski-term [23].

Expanding the LLGE, the STT for a thin film of thickness t and the polarization of the spin-magnetic moments $\vec{P}$ can be written as

$$\vec{T}_{\mathrm{STT}} = -\frac{\beta}{M_0}\vec{M} \times \vec{M} \times \vec{P} \tag{30}$$

where $\beta = j_c \frac{\epsilon}{g} \mu_{\mathrm{B}} 2eM_0 t$ with the spin-polarization efficiency ϵ gives the growth rate of the magnetization oscillations by the STT [2]. With this expansion the Landau-Lifshitz-Gilbert-Slonczewski equation (LLGSE) is given:

$$\frac{\partial \vec{M}}{\partial t} = \vec{T}_{\mathrm{H}} + \vec{T}_{\mathrm{G}} + \vec{T}_{\mathrm{STT}} \tag{31}$$

where $\vec{T}_{\mathrm{H}}$ is the torque from the LLE and $\vec{T}_{\mathrm{G}}$ is the additional Gilbert torque.
For easier application the STT can be approximately rewritten as Gilbert torque: Consider an infinite ferromagnet saturated by a magnetic field in z direction and a dynamic component of the magnetization $\vec{m}_{\sim} \ll M_0$ and a spin current polarized with $\vec{P} \parallel H$. Then the Gilbert torque can be approximated to

$$T_{\mathrm{G}} \approx -\alpha\omega_{\mathrm{H}}(\vec{m}_x + \vec{m}_y) \tag{32}$$

being colinear to

$$T_{\mathrm{STT}} \approx -\beta(\vec{m}_x + \vec{m}_y). \tag{33}$$

The STT could also be included in an effective damping parameter $\alpha' = \alpha - \frac{\beta}{\omega_{\mathrm{H}}}$, regaining the LLGE.

3 Experimental method and sample

In this chapter the examined sample is described and the experimental setup and method are explained.

3.1 Sample

The nano-wires studied here are made of multilayers of platinum (7 nm thickness), permalloy (5 nm) and aluminium oxide (<5 nm) on top and fabricated on a sapphire ground layer. The multilayers are created with sputtering and the wire pattern is created by electron-beam lithography. The active region is defined by the space of 1.8 µm between the leads consisting of a Chromium (7 nm) Gold (35 nm) bilayer.
The resulting nano-wire is 6 µm long with an active region of 1.8 µm and 180 nm wide. Figure 6 shows a scanning electron microscope (SEM) image of a sample.

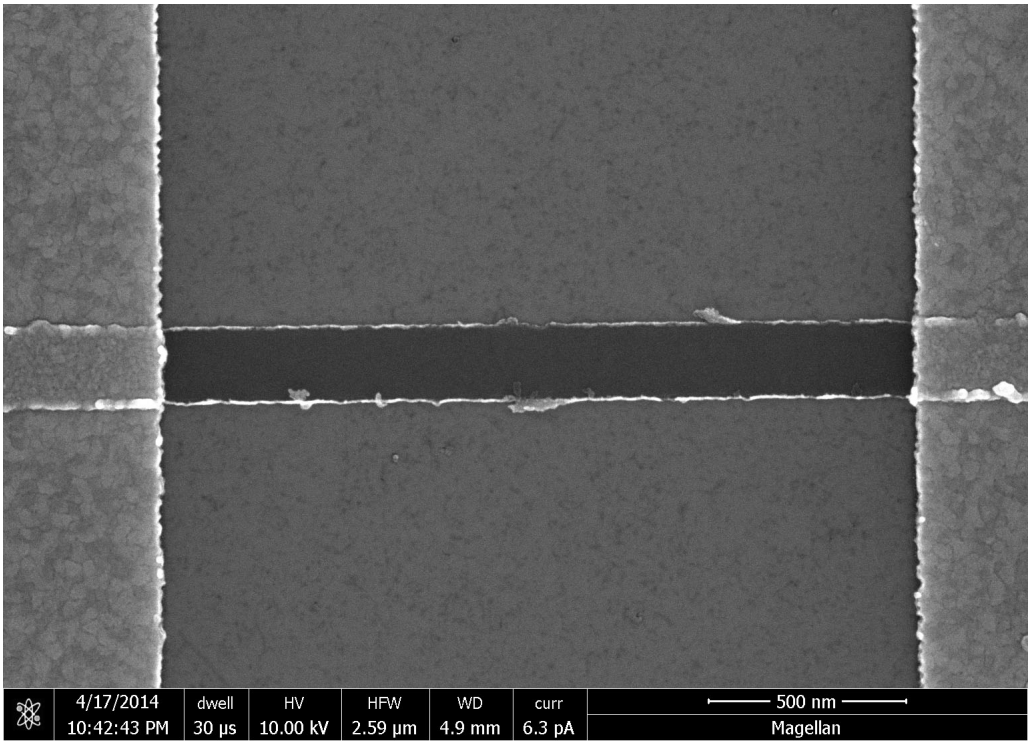

Figure 6: SEM image of a similiar sample.

3.2 Experimental method

The active region of the nano-wire mainly consists of the platinum and the permalloy layer. In the nonmagnetic Pt layer ~~the~~ SHE ~~effec~~t is used to create a spin current from a charge current. This spin current, being oriented transverse to the charge current, flows to the Pt/Py interface and excites spin torque oscillations in the magnetic Py layer. A saturating magnetic field ($H > 800$Oe) is applied in the plane of the sample and a direction nearly perpendicular to the axis of the nano-wire.

A direct current source provides the charge current I_{dc} that results in ~~the~~ SHE happening in the Pt layer. A bias tee is used to extract the microwave signal resulting from the FMR in the sample, which is registered by a spectrum analyzer.
The microwave spectrum is measured for different values of I_{dc} and H and different angles between the magnetic field direction and the nano-wire axis. By the variation of those parameters information about the behavior of magnetization oscillations and FMR in the nano-wire are obtained.

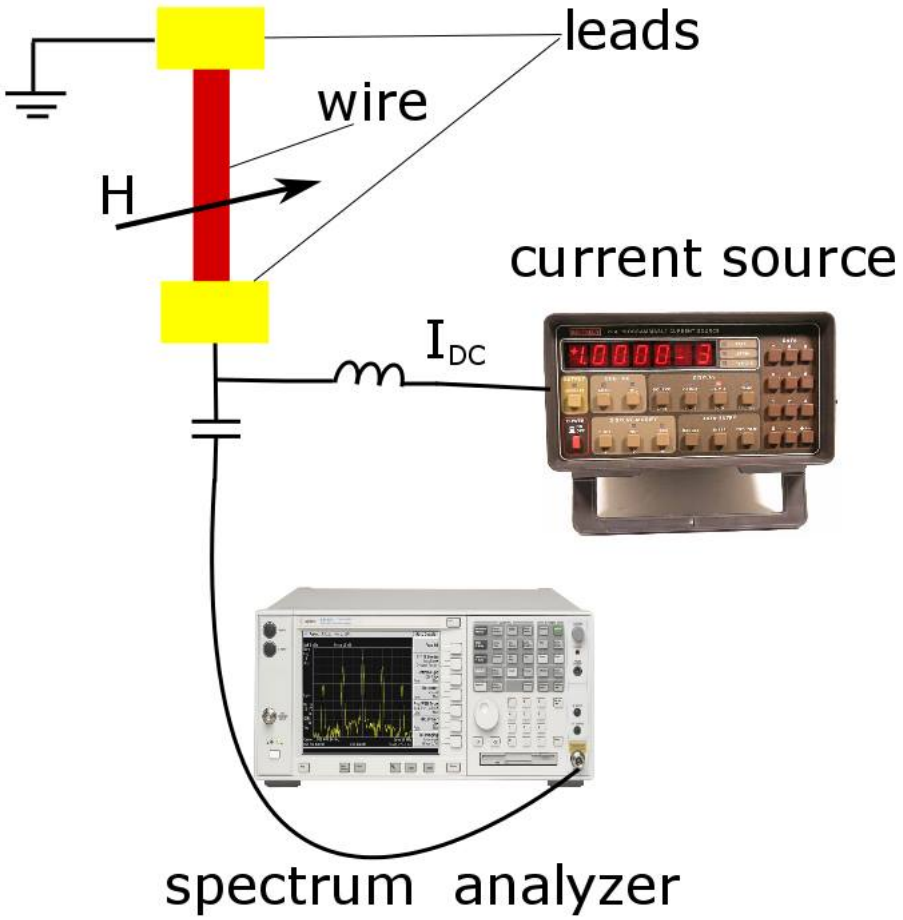

Figure 7: Experimental setup.

4 Experimental results

Here the experimental results are presented. To acquire knowledge about the magnetic oscillations in the nano-wire the behavior of the microwave spectrum was observed under various different angles θ and strengths of the magnetic field H and different currents I_{dc}. A typical microwave spectrum of the device for $\theta = 10°$, $H = 472\ Oe$ and $I_{dc} = 2.7\ mA$ is shown in figure 8.

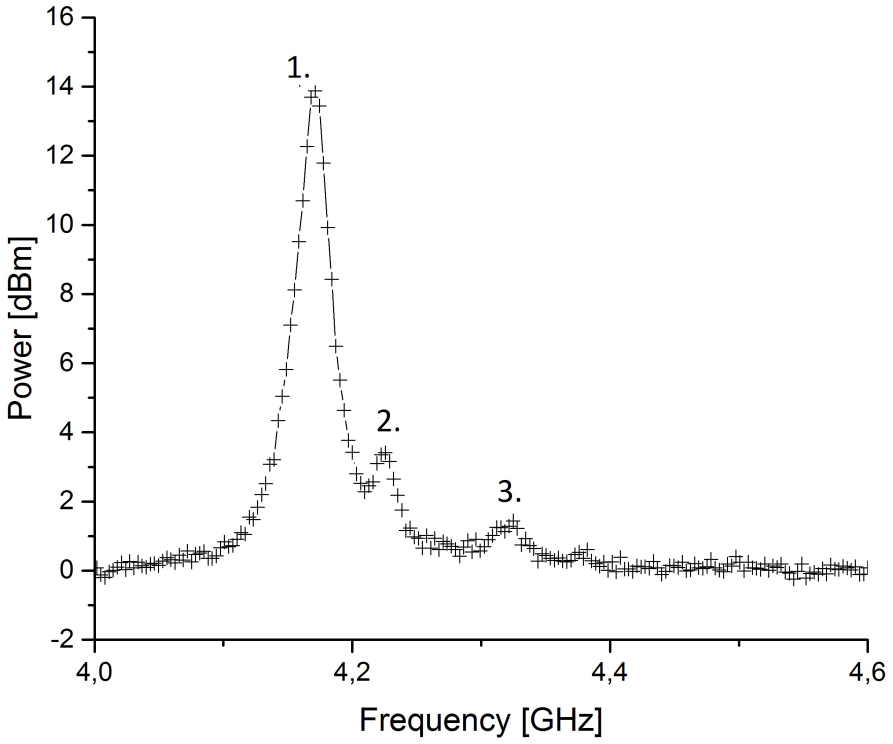

Figure 8: Expample of a microwave spectrum emitted by the sample at $\theta = 10°$, $H = 472$ Oe and $I_{dc} = 2.7$ mA. Curves are guides for the eyes.

There is a clear peak (1.) at the characteristic frequency of $f = 4.18$ GHz immediately followed by a second, smaller peak (2.). A third (3.) broader, even smaller peak can be seen at even higher frequencies. From micromagnetic simulations later in this thesis (section 5) we can see that none of these match the frequency of a bulk mode (see section 2.4).

A Lorentz fit gives a good approximation of the behavior of the microwave spectrum for the first edge mode. For future observations the microwave spectra will always be Lorentz fitted to make statements about maximum power, characteristic frequency f_0 and full width at half maximum (FWHM), which indicates the damping.

From theoretical considerations one would expect an ideal thin peak. The nonzero line width results from thermal fluctuations and nonlinear effects.

4.1 Dependence on the magnetic field direction

First measurements with variation of the magnetic field direction indicate a symmetric behavior with the angle Θ of the magnetic field, that gives the deviation from being perpendicular to the nano-wire axis. We can find the angle where the magnetic field is exactly perpendicular to the nano-wire axis. This angle is set to be $\Theta = 0$.
Now the optimal position for the magnetic field in perspective to the wire-axis had to be found. Therefore the magnetic field was rotated around the sample and the microwave spectrum was measured every 1°. After an initial saturating magnetic field of $H > 800$ Oe the magnetic field strength was set to $H = 522$ Oe. The electric current was set to $I_{dc} = 2.7$ mA and the angle was rotated in the area $-25° > \theta > 25°$. For each angle the maximum power and the frequency are presented in figure 9.

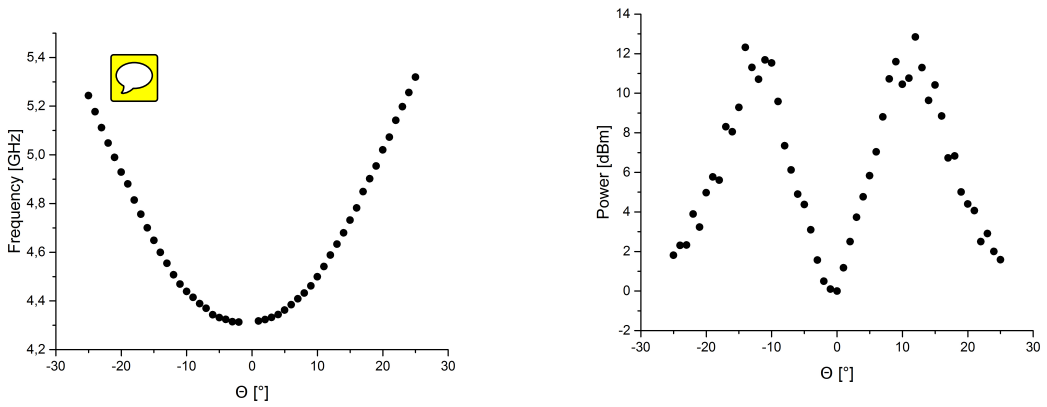

Figure 9: Signal power and frequency depending on the angle Θ.

First observations show that the system behaves mostly axisymmetrically at angles up to $\theta = 25°$. The maximum power can be achieved at the angles $\theta = -14°$ and $\theta = 12°$ and nearly vanishes for angles $|\theta| > 22°$ and $|\theta| < 2°$.
The symmetric behavior is expected and follows directly from the symmetry of the system. For angles below 2° the differential FMR is too low to show effect, while for angles over 22° the component perpendicular to the direction of the spin current becomes too weak.
To get reasonable results, in the following the angle will be set to $|\theta| = 10°$.

4.2 Dependence on the magnetic field strength

To find the field strength where the FMR is at its greatest, it was varied in an area 330 Oe $< H <$ 840 Oe with steps of $\Delta H = 8.38$ Oe. The charge current was set to $I_{\mathrm{dc}} = 2.7$ mA and the magnetic field direction was set to an angle of $\Theta = \pm\ 10°$. In Figure 10 the frequency, the power and the full width at half maximum (FWHM) of

the FMR-peaks are displayed.

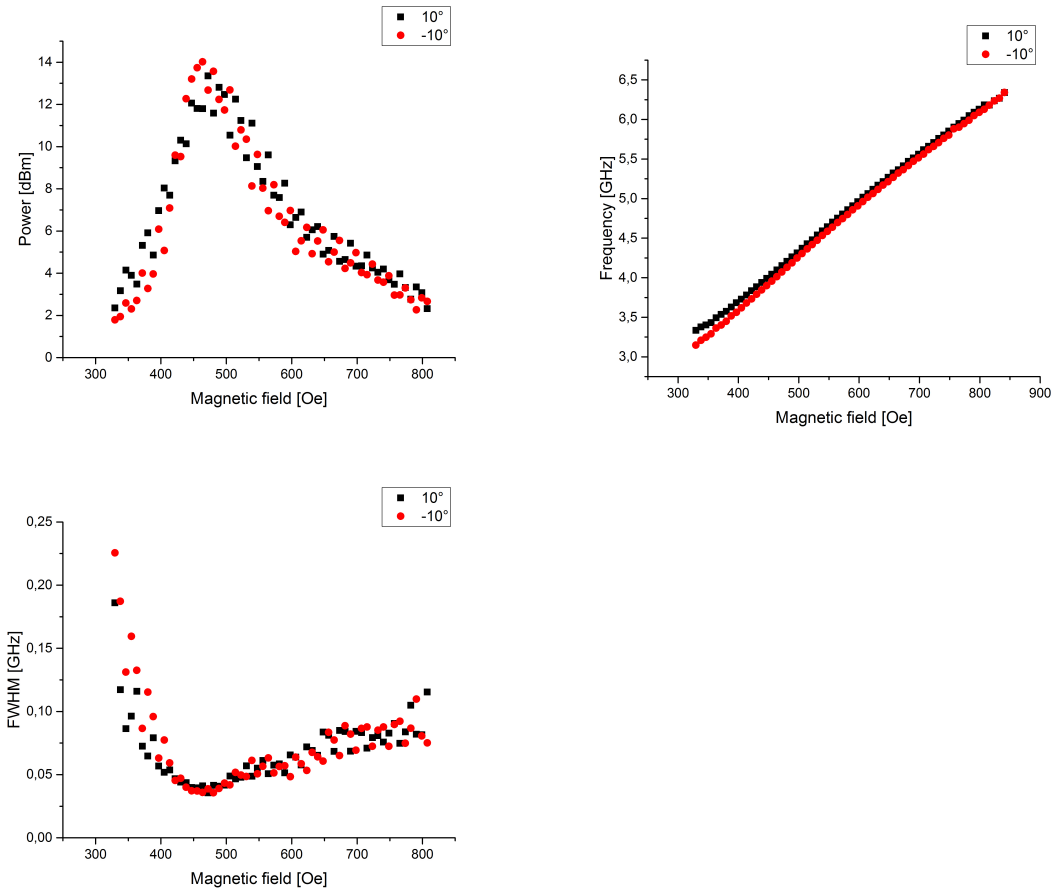

Figure 10: Signal power, frequency and FWHM depending on the magnetic field.

The frequency seems to increase linearly with the magnetic field, while the power shows a peak at around $H = 475$ Oe. The behavior of the FMR-power is asymmetric: at the left flank the power increases strongly with the magnetic field, while at the right flank it decreases much slower. This asymmetric behavior indicates that we observe the first mode of magnetic self-oscillations. At lower magnetic fields, meaning lower oscillation frequencies, the oscillation excitation from the SHE is not strong enough to work against the systems Gilbert-damping. At higher magnetic field strengths energy partially flows in the excitation of higher oscillation modes, which results in additional microwave signals while the signal from the first mode decreases. For low magnetic field strengths the peaks are very broad (high FWHM) and become the narrowest roughly at the same magnetic field where the peak height is at its maximum. For even higher fields they become broader again, but the FWHM increases much slower than it decreases at low fields.

For maximum signal powers the magnetic field should be set around 450 Oe $< H <$ 500 Oe.

4.3 Dependence on the direct current

The direct currents regulates the spin current generated by the SHE. In order to test the dependency of the system on the current we vary the current in an area 2.2 mA $> I_{dc} >$ 3.3 mA and measure the microwave spectrum at steps of 0.5 mA. The magnetic field is set to $H = 472$ Oe. Again, by lorentz-fitting the peak height, FWHM and the frequency are obtained and displayed in figure 11.

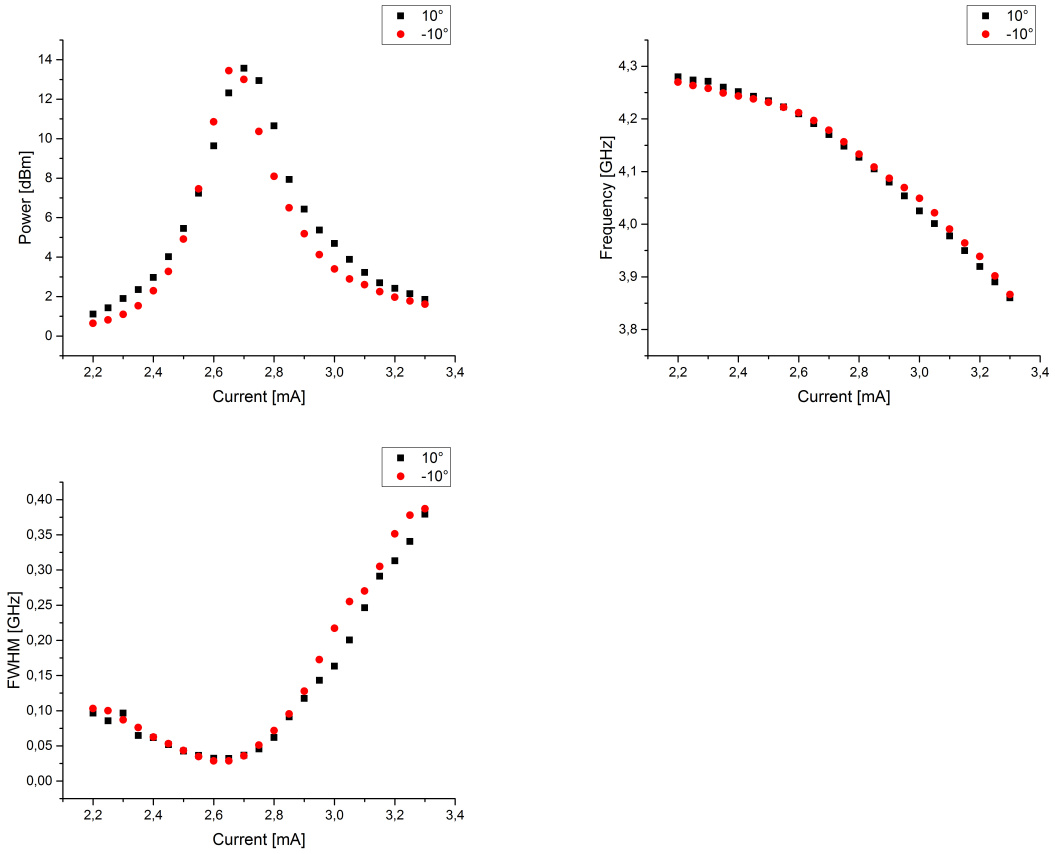

Figure 11: Signal power, frequency and FWHM depending on the direct current.

The power signal reaches a maximum value at $I_{dc} = 2.7$ mA, roughly at the same current where the peak width shows a minimum (lowest FWHM). The power of the signals at higher currents decreases slightly slower than it increases at lower currents. Also the peaks become much broader at higher currents. Below the critical current $I_{crit} = 2.2$ mA however, there is no FMR peak. This characterizes the minimum I_{dc} that is needed for the SHE to exceed the systems natural damping. Theoretically one would expect the FMR power to increase further with I_{dc}, but the nonlinear dynamic character of the system and effects such as four-magnon scattering ([24]) cap the FMR excitation at currents over 3.3 mA.

The FMR-frequency decreases with rising current, while it behaves nearly linearly at

lower currents (approximately until $I_{dc} = 2.4$ mA) and then decreases faster.

4.4 Resonant frequency at zero current

With the sample used in this thesis, a FMR-spectrum can only be detected with a current in the range 2.2 mA $> I_{dc} >$ 3.3 mA as seen in section 4.3. Since the resonant frequency varies with the current, we still need to obtain the resonant frequency at zero current because of the different critical current at different currents and to compare them to the results of micromagnetic simulation later. Therefor we assume linear behavior of the resonant frequency at lower currents and extrapolate the resonant frequency at zero current from the values we measured with $I_{dc} \leq 2.4$ mA (figure 14).

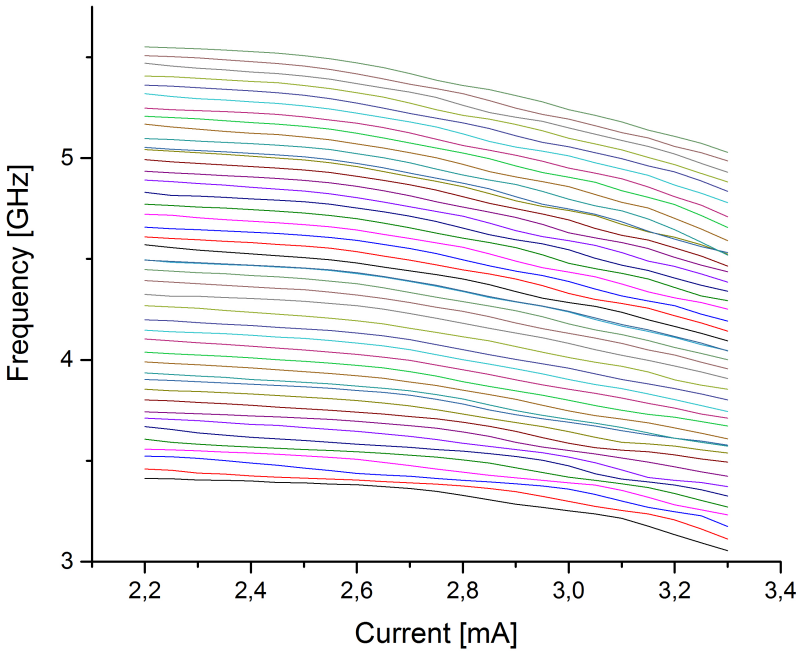

Figure 12: Frequency against current for different magnetic fields from $H = 250$ Oe to $H = 675$ Oe. $\Theta = 10°$.

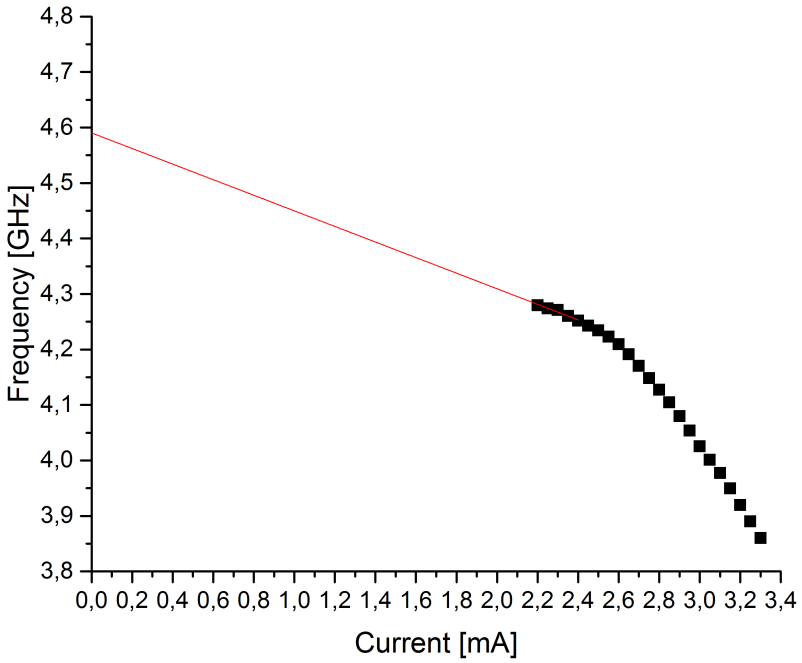

Figure 13: Example of the linear extrapolation.

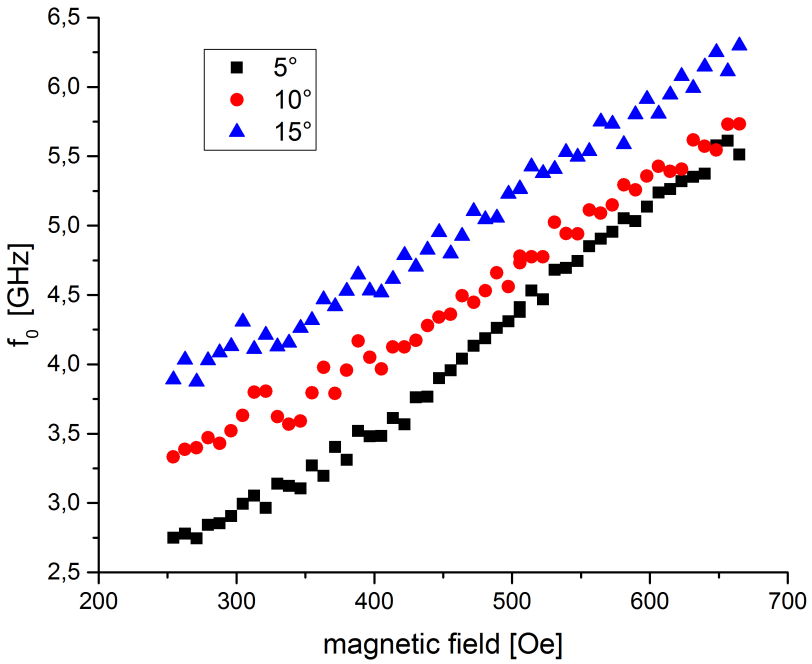

Figure 14: Calculated resonant frequencies at zero current for different magnetic fields H and angles Θ.

The current dependent frequency is measured for magnetic fields ranging from $H = 250$ Oe to $H = 675$ Oe and the resonant frequency at zero current is calculated by

extrapolation for three different angles $\Theta = 5°, 10°, 15°$.
We can see that the resonant frequencies extrapolated here follow roughly the same behavior as the measured frequencies in chapter 4.2. We can also see that the resonant frequency at zero current f_0 increases with the angle Θ, as expected from the measurements made in chapter 4.2.

5 Micromagnetic simulation

The theoretical description of magnetization dynamics in confined structures can often only be achieved by approximation of equations or for special cases (ellipsoid and its limiting cases[12]). Micromagnetic simulations give an alternate approach on a theoretical description by numeric integration of the LLGE.
In this chapter micromagnetic simulation will be used to obtain a model for our sample giving additional information about the magnetization dynamics. The program we are using is mumax^3 [25], which is a GPU-accelerated simulation program.

5.1 Basics of micromagnetic simulation

The principal concept of micromagnetic simulation is the fragmentation of a magnetic sample into cells whose behavior is given by the LLGE and the interaction with near or neighboring cells. Similar to the theoretical considerations in chapter 2 the quantum-mechanical origin of magnetism is only approximated by a mean field approximation [**?**]. With this method magnetization dynamics can be described on a time scale of ps and a spatial scale of nm, with upper limits given by computational time and memory.
To use micromagnetic simulation the sample geometry has to be broken to a number of $N = N_x N_y N_z$ cubic cells, this approach is called finite differences. These cells should have the same size, which should be of the order of the exchange length. For permalloy the exchange length was found to be 5.7 nm [26].
For each cell the contribution of each energy term to the effective field is calculated using discrete equations, each with different computational effort. All simulations in this thesis were done without taking into account thermal fluctuations ($T = 0$ K).

5.2 Sample and parameters

The sample in mumax^3 is represented by a cell grid. Since we want our simulation to represent the sample used in the experiments, grid size and cell size are chosen as follows: The simulated sample is 190 nm wide (x), 1.91 ţm long and 5 nm high. It consists of 38 cells in x-direction, 382 cells in y-direction and 2 cells in z-direction, resulting in cell sizes of 5 nm $\times$ 5 nm $\times$ 2.5 nm (figure 15). The size was chosen accordingly to the exchange length, while minimizing the used computation time.
To include the leads at each end of the sample, two additional cell grids of the same size are added, one at each side of the sample. Additionally, as described in section 2.1, the demagnetizing field is influenced by the samples boundaries. To minimize the influence of the demagnetizing field originating from the limitation of the simulation grid, periodic boundary conditions are introduced in y-direction, meaning that the simulation behaves as if the whole setting is repeated 5 times at each side of the sample in y-direction.

The saturation magnetization is set to be 600 Oe and the exchange stiffness is set to be $13 \cdot 10^{-12}$ J/m, both typical values for permalloy. The damping parameter α is exemplary set to be 0.0001 in the region of the nano-wire to get reasonable computation times without changing the behavior and 0 in the regions of the leads. The magnetic field is applied uniformly, its strength and direction can be varied while the angle of $\Theta = 0°$ coincides with the x-axis.

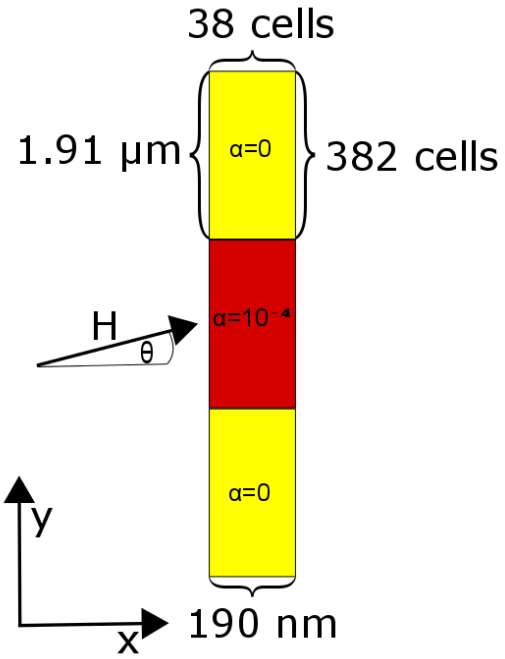

Figure 15: Shematic of the sample used in simulation.

5.3 Simulation

Like in the experiment magnetization oscillations are to be excited inside the sample. The first step in the simulation is to acquire a realistic ground state. Therefor the damping parameter is set to $\alpha = 1$, a very high value, and the simulation time runs for a time of 5 ns. After that short period of time the state of the system is saved as ground state, this state will later be subtracted to show the temporal behavior. For the following simulation α is set back to its original values.
The excitation by the STT in the experiment can not be simulated directly by mumax[3]. Instead we introduce an excitation by an additional external magnetic field in z-direction. To find the resonant frequency all frequencies of the chosen area have to be excited. We choose the magnetic excitation field to be a sinc function

$$H_{\text{exc}} = \frac{\sin\left(2\pi f_{\text{max}} t\right)}{2\pi f_{\text{max}} t} \tag{34}$$

with the time t and the maximum frequency $f_{\max}$ chosen to be 20 GHz. With its Fourier transformation being the rectangle function all frequencies with $f \leq f_{\max}$ are equally excited.

5.4 Simulation results

5.4.1 Ground state

In the simulation results for the ground state are as expected. Since the internal field is reduced at the edges by the demagnetizing field (chapter 2.1) and the magnetic field mainly points in x-direction, the x-component of the magnetization is also reduced at the edges while the y-component is greater at the edges (figure 16).

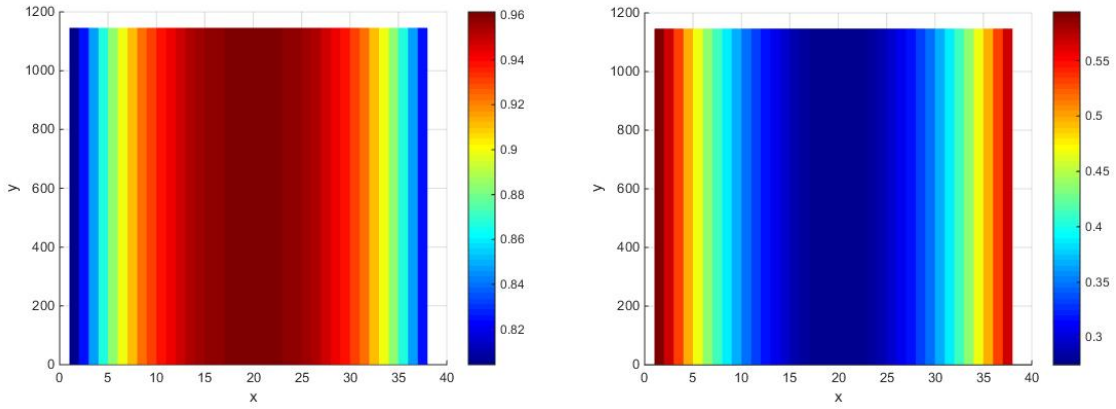

Figure 16: Components of the magnetization in ground state for $\Theta = 10°$ and $H = 700$ Oe for each cell. Left: x-component, right: y-component.

5.4.2 Data processing

To acquire information about the magnetization oscillation excited in the nano-wire, the time behavior of the magnetization inside the sample is analyzed. Each component of the magnetization and its behavior in the time space can be extracted from the simulation data. With a Fourier transformation the behavior of each magnetization component in the frequency space can be obtained. For each frequency then one can infer the oscillation amplitude in the whole sample at this frequency by finding the amplitude in each cell for the chosen frequency. In figure 17 these steps of data processing are illustrated.

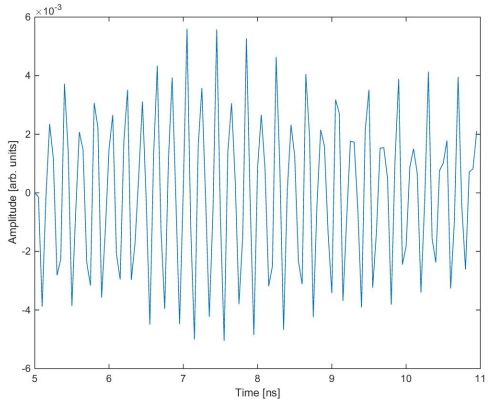

(a) Time dependent behavior of the y-component of the amplitude in an example cell.

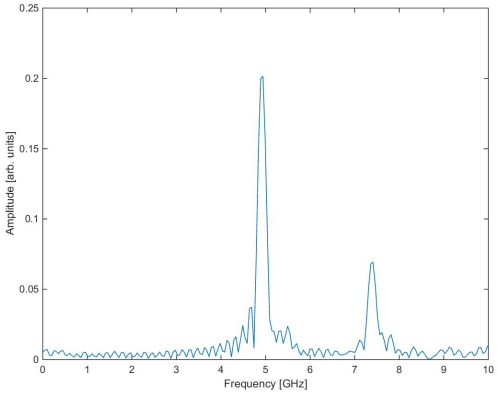

(b) Frequency spectrum of the same cell obtained via Fourier analysis. The maximum is at $f = 4,941$ GHz.

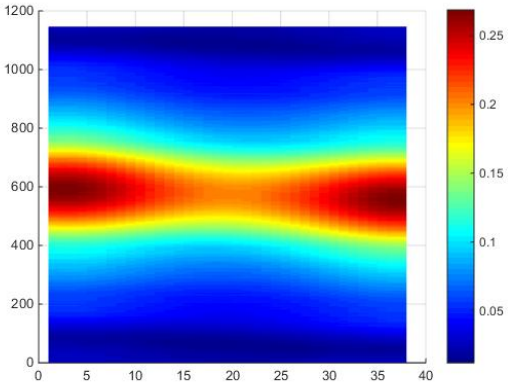

(c) y-component of the amplitude for oscillations at the frequency $f = 4.941$ GHz.

Figure 17: Data processing on the example of a field strenght $H = 600$ Oe at $\Theta = 10°$.

5.4.3 Dynamics

In the experiments the frequency spectrum always showed at least two peaks. In the spectra obtained by the simulation there are always exactly two peaks as it can be seen in figure 18 for different magnetic field strength.

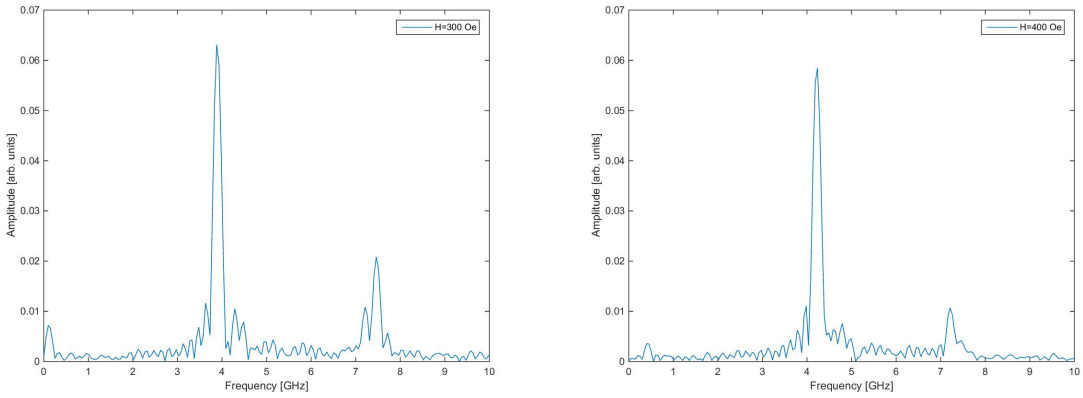

(a) 300 Oe

(b) 400 Oe

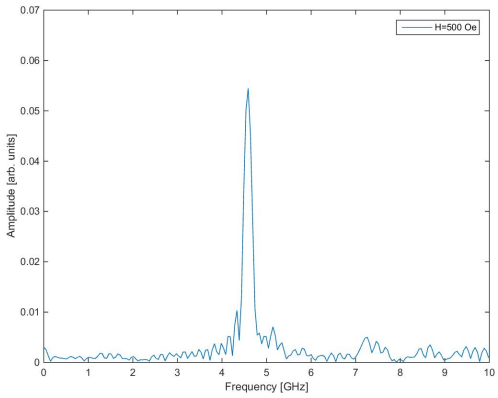

(c) 500 Oe

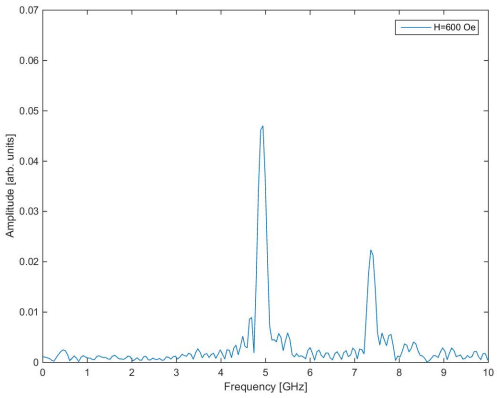

(d) 600 Oe

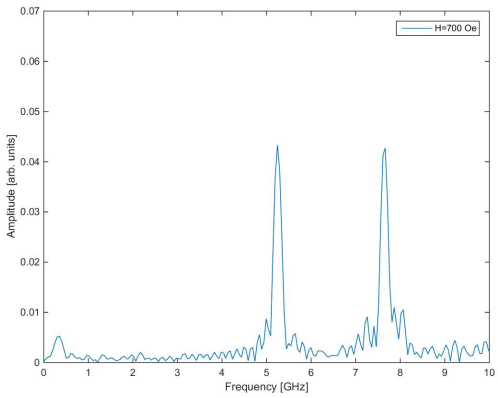

(e) 700 Oe

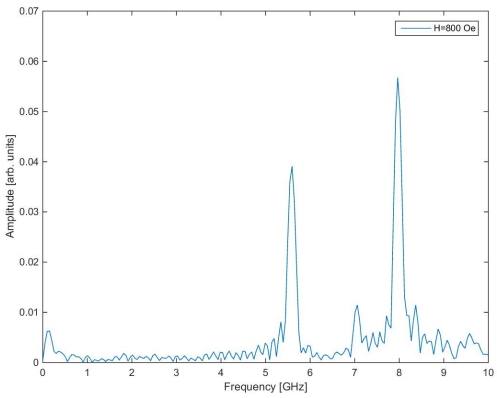

(f) 800 Oe

Figure 18: Spectrum of the z-component of the amplitude for different external magnetic fields obtained by micromagnetic simulation.

We can again identify the peak at lower frequencies as edge mode and the peak at higher frequencies as bulk mode. The edge mode peak has its maximum at a frequency of $f = 4.941$ GHz, an example of the corresponding amplitudes is shown in figure 19 (y-component can be found in figure 17c) for $H = 600$ Oe and $\Theta = 10°$.

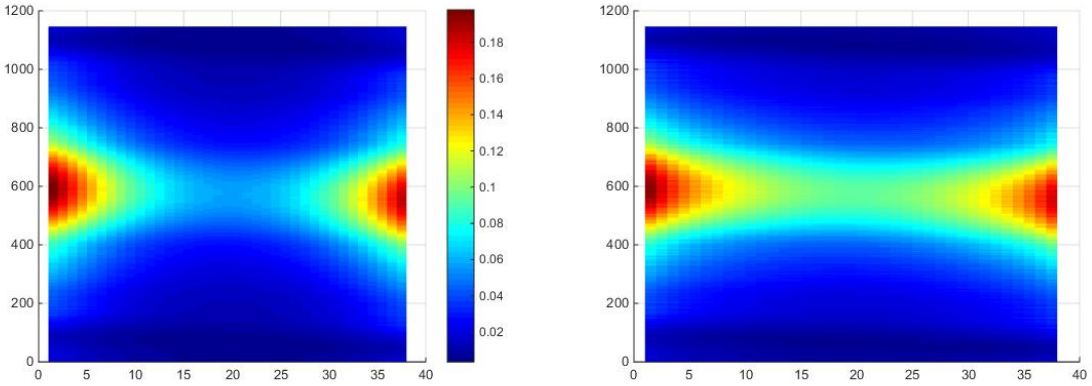

(a) x-component (b) z-component

Figure 19: Components of the oszillation amplitude at $f = 4.941$ GHz with $H = 600$ Oe and $\Theta = 10°$ (y-component can be found in figure 17c).

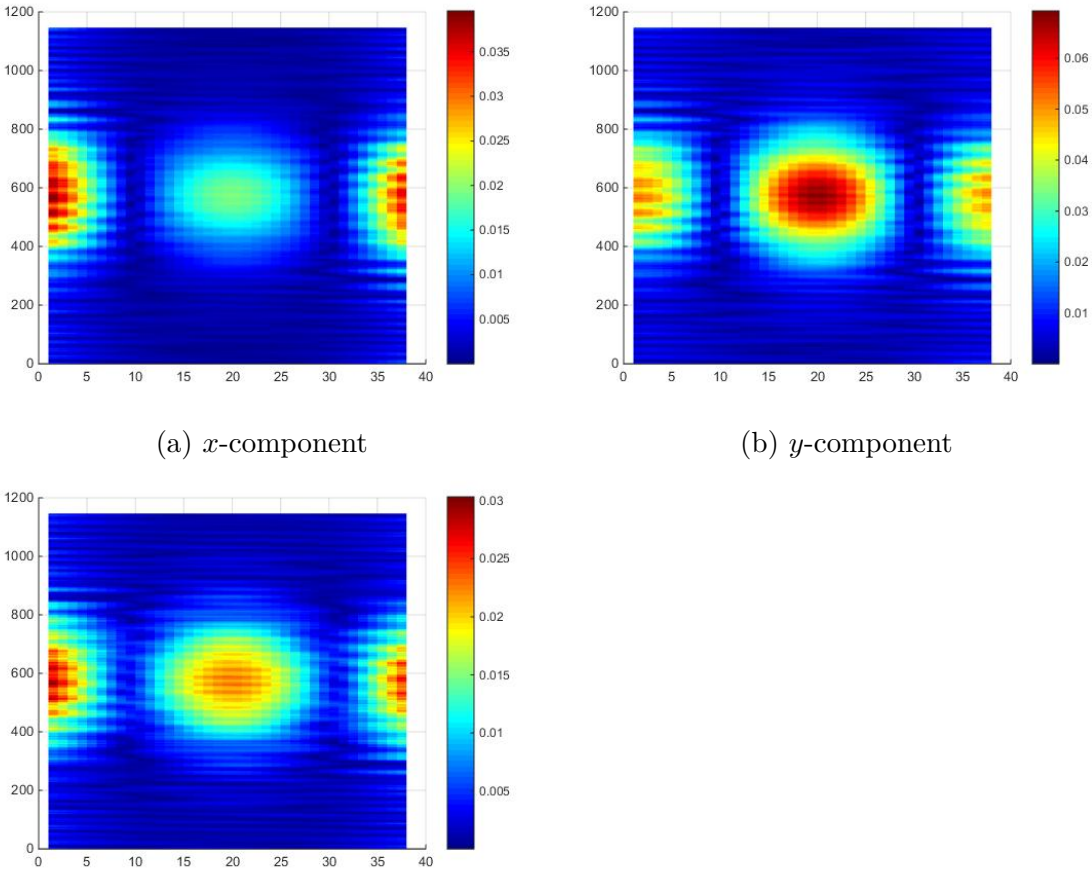

(a) x-component (b) y-component

(c) z-component

Figure 20: Absoulute values of the components of the oszillation amplitude at $f = 4.941$ GHz with $H = 600$ Oe and $\Theta = 10°$.

One can see that the amplitudes are highest (and so the oscillations are strongest) at the edges of the nano-wire and get reduced going to the center.

At the frequency of $f = 7.361$ GHz the bulk mode peak has its maximum. The corre-

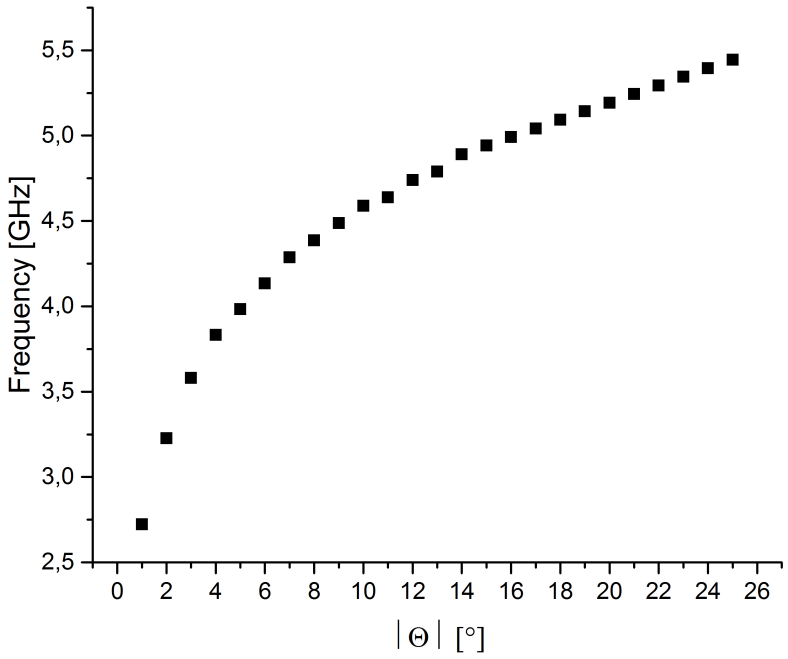

Figure 21: Frequency of the edge mode in dependence of the angle Θ taken from simulation data.

sponding amplitudes are displayed in figure 20. Here we have the strongest oscillations split, being partially in the center region and partially also at the edges of the nanowire. We find that these oscillations have a different sign at the center than the ones at the edges. This suggests that we do not have a „pure“bulk mode, but a superposition of bulk and edge mode.

Varying the direction of the external magnetic field it is found that the system behaves perfectly symmetric according to the frequency of the edge mode (figure 21) as already seen in the experiments.

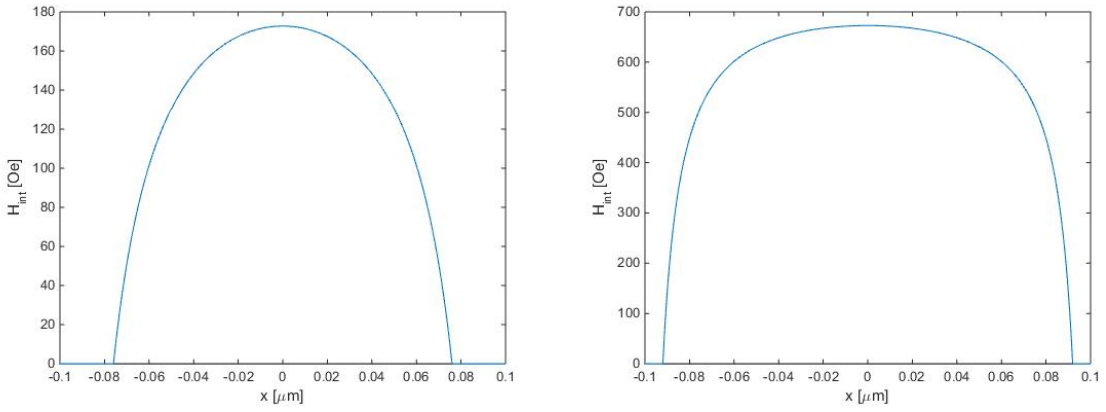

(a) $H = 300$ Oe (b) $H = 800$ Oe

Figure 22: Internal magnetic field at external fields H.

For lower strengths of the external magnetic field the internal magnetic field also changes not only in strength, but also in form (figure 22). At the field strength of $H = 300$ Oe the region where $H_{\text{int}} = 0$ Oe is much broader than for example at $H = 800$ Oe. This also affects the magnetization oscillation within the sample. In figure 23 the z-component of the amplitude is shown for different magnetic fields. For low magnetic fields the oscillations are mainly located at the center of the sample. For increasing magnetic fields the region where the magnetic field is zero inside the sample reduces and the oscillations move to the edges.

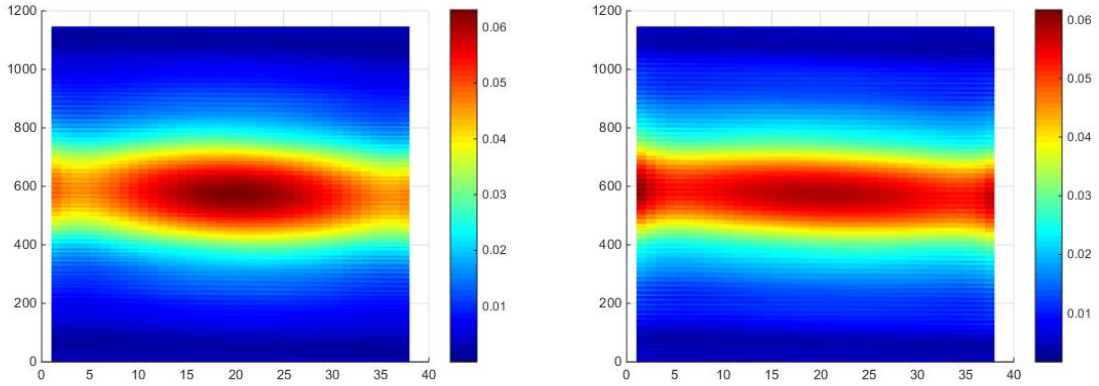

(a) $H = 300$ Oe

(b) $H = 400$ Oe

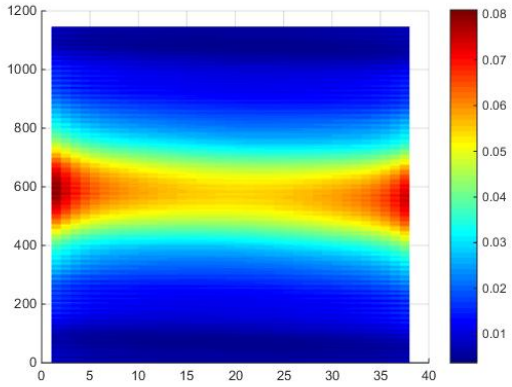

(c) $H = 500$ Oe

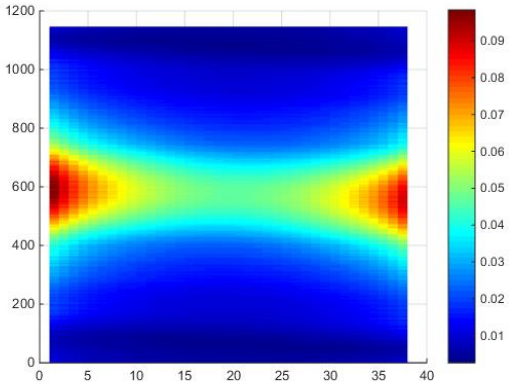

(d) $H = 600$ Oe

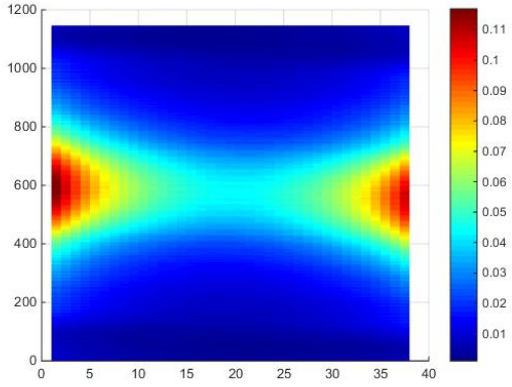

(e) $H = 700$ Oe

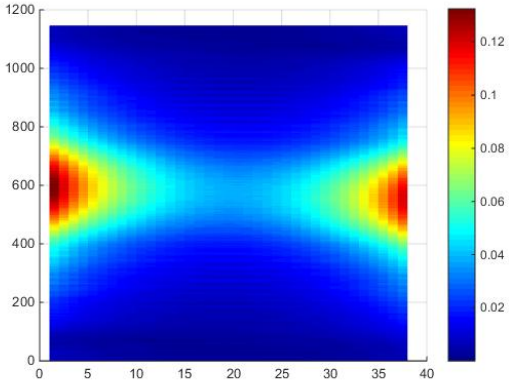

(f) $H = 800$ Oe

Figure 23: z-component of the oscillation amplitude at different magnetic fields.

The frequency of the edge mode obtained by the simulation can be directly compared to the frequency at zero current obtained by the experiment. For the angles $\Theta = 5°, 10°, 15°$ the frequencies of the edge mode for different magnetic fields in the area 200 Oe $\leq H \leq$ 750 Oe are determined (figure 24).

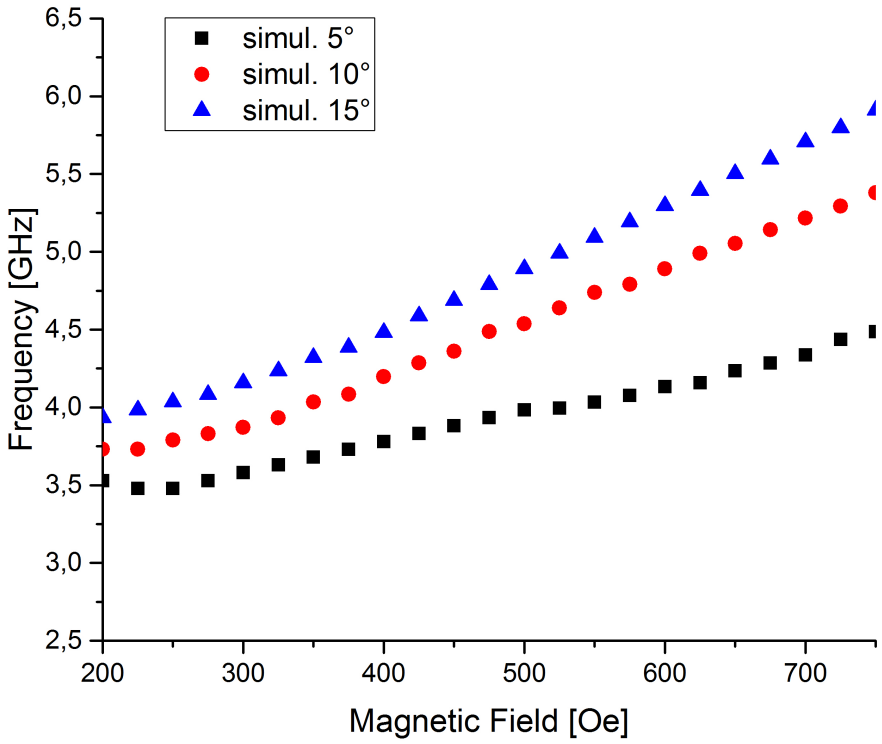

Figure 24: Frequency of the edge mode determined from simulation.

We can see that the dependence on the angle Θ and the magnetic field H roughly matches the behavior we found in the experiment (figure 14),even though they only match qualitatively. This confirms that the oscillations observed in the experiment actually are oscillations in the edge regions of the nano-wire.

6 Discussion

In this section the results from the experiment and the micromagnetic simulations are compared and discussed.

We found that magnetization oscillation can be excited inside the nano-wire as active region demonstrating that it is possible to excite self-oscillatory dynamics by spin-orbit (SO) torques in an extended region. This opposes recent experiments [27], that showed that uniform application of SO torques on an extended ferromagnetic film does not excite magnetic self-oscillations because of nonlinear magnon scattering processes. In [28] it is argued that the quantization inside the nano-wire geometry reduces the effect of those nonlinear magnon scattering processes. As a result enables the excitation of self-oscillatory magnetization dynamics inside the sample. Four-magnon scattering for example can be suppressed by a geometry that is narrower than a critical width, which is given by the four-magnon scattering wave vector [24]. For a 5 nm thick permalloy nano-wire this width is about 0.5 μm [28].

The frequency spectrum found in the experiments has one major peak and, depending on the chosen parameters, up to two smaller peaks (figure 8). In contrast the simulation shows two clear peaks, one for the edge mode and one for the bulk mode. Comparing the frequencies at which those peaks can be found we can conclude that all peaks found in the experiments are harmonics of the edge mode, the bulk mode could not be measured at any frequency or magnetic field. This suggests that the bulk mode is not excited in the sample at all and all energy is absorbed by edge modes.

The experimental setup shows a nearly symmetrical behavior considering the angle Θ (figure 9). It can be seen that the microwave signal originating from the FMR can only be measured for angles $2° \leq |\Theta| \leq 25°$. For lower angles the effect of the differential FMR is too low to be measured while for larger angles the component of the magnetic field perpendicular to the nano-wire axis becomes too small. In the simulation also a symmetrical behavior was observed. However, the behavior of the frequency showed a different form than the measured data. The reason for the difference in behavior probably comes from the nonzero direct current at which the experimental data was obtained.

The dependence on the magnetic field showed a maximum amplitude at a external magnetic field of $H = 475$ Oe (figure 10). For field lower than $H = 300$ Oe no FMR intensity could be measured since the signal becomes too small (see section 2). At magnetic field strengths larger than $H = 500$ Oe the FMR intensity decreases again. Because of the the broader FMR peaks at those magnetic field strengths we argue that instead of the first harmonic edge mode higher modes are excited. In the simulation instead we observed that the edge mode peak becomes smaller with increasing magnetic field strength while the bulk mode peak at first also decreases and then for fields larger than $H = 450$ Oe increases again.

For the dependence on the SHE controlling direct current we found that a critical current has to be reached to exceed the Gilbert-damping factor and to excite self-oscillatory magnetization dynamics. It was also found that the maximum FMR amplitude corresponds to a current of $I_{\mathrm{DC}} = 2.7$ mA. For larger currents nonlinear magnon scattering effects suppress excitation of self-oscillatory dynamics.
The resonant frequencies at zero current show the same behavior with external magnetic field direction and strength as found before (figure 14). They match with the findings from the simulation for resonant frequencies showing that the oscillation modes measured in the experiment indeed are edge modes as the ones observed in simulation. For all experimental data it must be considered that the sample did not have a perfect smooth shape due to the creation process.
As a conclusion self oscillations excited by STT could be measured in a nano-wire as a nearly one-dimensional structure and the measurement result match the theoretical results obtained from micromagnetic simulation for the most part.

Acknowledgement

While working on this thesis I have benefited greatly from the support of many people, some of whom I would like to thank here.
First, I am deeply grateful to my advisor Dr. Vladislav Demidov who dedicated a lot of time to introduce me to the field of magnonics and to answer my numerous questions while also discussing results with me.
I would like to thank Prof. Dr. Sergej Demokritov for accepting me into his work group and offer me a topic for my bachelor thesis I am really interested in.
Also I am thankful to Dr. Johann Jersch for initially sparking my interest in the field of magnonics.
For a warm welcome and a pleasant working experience I would like to thank all members of the work group Nonlinear Magnetic Dynamics, especially Michael Evelt for being helpful with every kind of problem I was confronted with during my work and for proofreading the whole thesis.
Last but not least i would like to thank my family, friends and my fellow students, especially Arne Hörmeyer and Yvonne Krummbeck for proofreading the thesis.

Bibliography

[1] P. Seibt, "Parametric excitation of spin waves in permalloy nanoellipses," 2012.

[2] H. Ulrichs, "Spin-wave instabilities on the nanoscale," 2014.

[3] M. N. Baibich and J. M. Broto, "Giant Magnetosresistance of (001)Fe/(001)Cr Magnetic Superlattices," *Physical Review Letters*, vol. 61, no. 001, pp. 2472–2475, 1988.

[4] G. Binasch, P. Grünberg, F. Saurenbach, and W. Zinn, "Enhanced magnetoresistance in layered magnetic structures with antiferromagnetic interlayer exchange," *Physical Review B*, vol. 39, no. 7, pp. 4828–4830, 1989.

[5] T. Miyazaki and N. Tezuka, "Giant magnetic tunneling effect in Fe/Al2O3/Fe junction," *Journal of Magnetism and Magnetic Materials*, vol. 139, no. 3, pp. L231–L234, 1995.

[6] F. Bloch, "Zur Theorie des Ferromagnetismus.," *Zeitschrift für Physik*, vol. 6, pp. 206 – 219, 1930.

[7] V. V. Kruglyak, S. O. Demokritov, and D. Grundler, "Magnonics," *Journal of Physics D: Applied Physics*, vol. 43, no. 26, p. 264001, 2010.

[8] S. I. Kiselev, J. C. Sankey, I. N. Krivorotov, N. C. Emley, R. J. Schoelkopf, R. A. Buhrman, and D. C. Ralph, "Microwave oscillations of a nanomagnet driven by a spin-polarized current.," *Nature*, vol. 425, no. 6956, pp. 380–383, 2003.

[9] W. H. Rippard, M. R. Pufall, S. Kaka, S. E. Russek, and T. J. Silva, "Direct-current induced dynamics in Co90 Fe10/Ni80 Fe20 point contacts.," *Physical review letters*, vol. 92, no. 2, p. 027201, 2004.

[10] V. E. Demidov, S. Urazhdin, E. R. J. Edwards, and S. O. Demokritov, "Wide-range control of ferromagnetic resonance by spin Hall effect," *Applied Physics Letters*, vol. 99, no. 17, pp. 2013–2016, 2011.

[11] S. Neusser and D. Grundler, "Magnonics: Spin waves on the nanoscale," *Advanced Materials*, vol. 21, no. 28, pp. 2927–2932, 2009.

[12] A. G. Gurevich and G. A. Melkov, "Magnetization oscillations and waves," p. 464, 1996.

[13] C. Kittel, "On the Theory of Ferromagnetic Resonance Absorption," vol. 460, no. 1946, 1948.

[14] C. Kittel, *Einführung in die Festkörperphysik*. Oldenburg Wissenschaftsverlag, 1953.

[15] T. Gilbert, "Classics in Magnetics A Phenomenological Theory of Damping in Ferromagnetic Materials," *IEEE Transactions on Magnetics*, vol. 40, no. 6, pp. 3443–3449, 2004.

[16] R. I. Joseph and E. Schlömann, "Demagnetizing field in nonellipsoidal bodies," *Journal of Applied Physics*, vol. 36, no. 5, pp. 1579–1593, 1965.

[17] B. A. Kalinikos and A. N. Slavin, "Ferromagnetic Films With Mixed Exchange Boundary," *J. Phys. C: Solid State Phys.*, vol. 19, pp. 7013 – 7033, 1986.

[18] M. I. D'yakonov and V. I. Perel', "Possibility of orienting electron spins with current," 1971.

[19] J. E. Hirsch, "Spin Hall Effect," p. 22, 2006.

[20] A. Hoffmann, "Spin hall effects in metals," 2013.

[21] L. Liu, T. Moriyama, D. C. Ralph, and R. a. Buhrman, "Spin-torque ferromagnetic resonance induced by the spin Hall effect," *Physical Review Letters*, vol. 106, no. 3, pp. 1–4, 2011.

[22] A. Manchon, "Spin Hall effect versus Rashba torque: a Diffusive Approach," p. 7, 2012.

[23] J. C. Slonczewski, "Current-driven excitation of magnetic multilayers," *Journal of Magnetism and Magnetic Materials*, vol. 159, no. 1-2, pp. L1–L7, 1996.

[24] H. Schultheiss, K. Vogt, P. Pirro, T. Brächer, P. A. Beck, and B. Hillebrands, "4 . 6 Four-magnon scattering in spin-wave micro-conduits," no. 2, pp. 51–55.

[25] A. Vansteenkiste, J. Leliaert, M. Dvornik, F. Garcia-Sanchez, and V. Waeyenberge

[26] J. Ha, R. Hertel, and J. Kirschner, "Micromagnetic study of magnetic configurations in submicron permalloy disks," *Physical Review B*, vol. 67, no. 22, pp. 1–9, 2003.

[27] V. E. Demidov, S. Urazhdin, E. R. J. Edwards, M. D. Stiles, R. D. McMichael, and S. O. Demokritov, "Control of magnetic fluctuations by spin current," *Physical Review Letters*, vol. 107, no. 10, pp. 1–5, 2011.

[28] A. Smith, Z. Duan, and L. Yang, "Nanowire Spin Torque Oscillator Driven by Spin Orbit Torques," *Bulletin of the American ...*, pp. 1–10, 2014.

Plagiatserklärung

Hiermit versichere ich Tim Bexter, dass die vorliegende Arbeit mit dem Titel “Study of nano-wire spin-Hall nano-oscillators” selbstständig verfasst worden ist, dass keine anderen Quellen und Hilfsmittel als die angegebenen benutzt worden sind und dass die Stellen der Arbeit, die anderen Werken - auch elektronischen Medien - dem Wortlaut oder Sinn nach entnommenen wurden, auf jeden Fall unter Angabe der Quelle als Entlehnung kenntlich gemacht worden sind.

Münster, 24. August 2015

Ich erkläre mich mit einem Abgleich der Arbeit mit anderen Texten zwecks Auffindung von Übereinstimmungen sowie mit einer zu diesem Zweck vorzunehmenden Speicherung der Arbeit in eine Datenbank einverstanden.

Münster, 24. August 2015